Author Manuscript

Author Manuscript

Author Manuscript

Author Manuscript

HHS Public Access

Author manuscript

Sens Biosensing Res. Author manuscript; available in PMC 2018 November 28.

Published in final edited form as:

Sens Biosensing Res. 2018 November ; 21: 65–74. doi:10.1016/j.sbsr.2018.10.005.

Object motion detection based on passive UHF RFID tags using a hidden Markov model-based classifier

Young Ho Lee[*] and **Ivan Marsic**

Electrical and Computer Engineering Department, Rutgers University, 94 Brett Road, Piscataway, NJ 08854, USA

Abstract

We present an object motion detection system using backscattered signal strength of passive UHF RFID tags as a sensor for providing information on the movement and identity of work objects—important cues for activity recognition. For using the signal strength for accurate detection of object movement we propose a novel Markov model with continuous observations, RSSI preprocessor, frame-based data segmentation, and motion-transition finder. We use the change of backscattered signal strength caused by tag's relocation to reliably detect movement of tagged objects. To maximize the accuracy of movement detection, an HMM-based classifier is designed and trained for dynamic settings, and the frequency of transitions between stationary/moving states that is characteristic for different object types. We deployed a RFID system in a hospital trauma bay and evaluated our approach with data recorded in the trauma room during 28 simulated resuscitations performed by trauma teams. Our motion detection system shows 89.5% accuracy in this domain.

Keywords

UHF RFID tags; HMM classifier; Motion detection

1. Introduction

For context-aware systems in indoor work settings, several types of sensors have been applied to capture work activities. Passive RFID tags have been used in various environments for monitoring object use because of their unique advantages compared to other sensors, such as active RFID tags, accelerometers, and computer vision. Passive RFID technology provides small tag sizes, suitable for different shapes and sizes of objects in work settings. Unlike accelerometers, passive tags operate without batteries and require no maintenance, and are cost-effective and readily applicable to most items including disposable ones. Computer vision has similar characteristics but raises privacy concerns, particularly in hospital settings. Vision is also less sensitive to small and randomly oriented objects of various shapes [1]. We focus on motion detection of used objects as a basis for activity recognition in indoor work settings. Our target application domain is the fast-paced,

This is an open access article under the CC BY-NC-ND license (http://creativecommons.org/licenses/BY-NC-ND/4.0/).

[*]Corresponding author: young2059@hotmail.com (Y.H. Lee).

Author Manuscript Author Manuscript Author Manuscript Author Manuscript

high-risk environment of trauma resuscitation. Such environments can benefit from context awareness about the currently performed activity. While most active devices and instruments in medical settings such as vital sign monitors, pulse oximeters, and anesthesia machines provide valuable information with physiological data [2], passive devices and tools, such as bag-valve mask (BVM), cervical collar, and CO_2 detector, need additional sensors to capture information about their use [3]. Detecting the motion and identity of such objects can serve as reliable cues about current work activities because most medical objects are uniquely associated with different tasks [4].

In this paper, we present a detection system for providing information on moving and stationary states of passive medical objects used on a patient bed of a trauma bay using passive ultra-high frequency (UHF) RFID technology. Important properties of our system are nonintrusive operation and preserving the privacy of medical teams. For the nonintrusive and privacy-preserving system, we employ the passive UHF RFID tags, whose working range is up to 11 m. This long range allows RFID reader antennas to be mounted onto the ceiling above the work are. The maximum range of 11 m is sufficient to interrogate tags from the reader antenna on the ceiling since the height of ceiling is typically no > 3 m. To detect movement of medical objects, the received signal strength indication (RSSI) of the tag is used. RSSI is RFID reader measurement of the power in received radio signals from an RFID tag. Since the strength of the received signal varies with the location and orientation of the tag [5], RSSI is a good indicator for detecting movement of tagged objects. When tag's location or angle are changed relative to the reader antenna, the tag's RSSI at the new location will be different from that at the previous location.

In developing a practical system, there are substantial challenges involved: (1) RSSI measurement tends to be significantly affected by the thermal noise at the reader side which results in ambiguous measurement because RSSI directly depends on weak backscattered signal power from the tag. The power of the backscattered signal is typically0.1 to 10 mW at the reader [6]. (2) Although the distribution of RSSI is often assumed as Gaussian [7,8], practically measured RSSI distributions are different from Gaussian due to unpredictable indoor propagations including constructive and destructive interference [6]. These varying distributions should be addressed in stochastic processing on RSSI. (3) RSSI measurement from a fast-moving tag over a short interval yields insufficient information on a moving state because the RFID system suffers from severe query-loss [9,10] resulting in lacking of the number of data samples to process noisy RSSI. (4) The device diversity in RSSI measurement causes extra amplitude in RSSI. Different RFID tags, readers and antennas, even from the same vendor, have different characteristics. Calibration of those devices would be impractical. Thus the diversity factors in RSSI measurement should be addressed when using RSSI from multiple devices. (5) Trauma rooms are crowded with people moving around the area of interest, causing interference to radio signals [4] and resulting in noisy RSSI.

We developed a detection system tackling the above challenges. To tackle Challenge (1) and (2), investigating distributions of RSSI and read rates of multiple tags in the area of interest, the patient bed, we designed RSSI preprocessor to reduce the variance of RSSI distribution introduced by the thermal noise and indoor propagation and make RSSI distribution closely

Author Manuscript Author Manuscript Author Manuscript Author Manuscript

follow Gaussian. Due to Challenge (3) we focus on the change caused by its relocation, rather than information from the moving tag. We introduce frame based segmentation of RSSI data to detect RSSI change and use it for observations of the HMM classifier. Since the HMM classifier makes movement detection on a frame basis, we develop motion-transition finder to determine the exact movement time within a frame based period. To tackle Challenge (4) we create a feature to compensate diversity terms. we use difference of RSSI based on a frame basis rather than using absolute RSSI values. By differentiating RSSI values of two consecutive frames, common extra amplitude of each frame RSSI introduced by diversity factors can be eliminated. To tackle Challenge (5), we develop an HMM classifier based on machine learning. In addition to the interference, each of medical objects has its own usage and frequency of being used so we use distinct parameters of the classifier for each object to train for maximizing the margin between different classes in the presence of the interference caused by human moving. Then we develop an augmented HMM classifier from the naive one to increase detection performance further. All details are elaborated in Section 3.

We make the following contributions: First, we investigate distributions of RSSI in the indoor environment and find out that the distributions randomly vary with locations and have large variances. We propose RSSI preprocessor that process RSSI to be reliable in distinguishing tag's motion and make accurate approximations to the Gaussian distribution for statistical processing. Second, for the detection system we present a novel method of constructing Markov models with continuous observations, introducing frame based data segmentation and motion-transition finder. The method results in a decrease in detection error rate by 10.8% compared to naive HMM. Third, we install a RFID system in a hospital trauma bay and evaluate the detection system. This result indicates that the passive UHF RFID tag is a new source of providing not only identification of medical objects but also information on their movement for context-aware systems in hospital settings. The rest of this paper is organized as follows. We review related work in Section 2. In Section 3, we present effects of Multiple tag interrogation and the design of RSSI preprocessor, HMM classifier and motion-transition finder. In Section 4, system hardware, tagged medical objects and experimental results are presented. Finally, we discuss the conclusions in Section 5.

2. Related work

In activity and motion recognition several types of sensor such as vision [11,12], accelerometer [13], and RFID tag [2,14] have been used. Although vision-based sensors are not intrusive to medical teams and provides rich contextual information, they raise privacy concerns in the medical domain of our context [8]. Compared to RFID tags whose information is affected by indoor propagation, physical accelerometer data are earned directly though hardwire, so accelerometers are not subject to indoor propagation. They however requires batteries and circuitry to work with considerable sizes, resulting in inapplicable to sensitive and small medical objects. Thus the passive RFID tag is decided to use in our system.

Author Manuscript Author Manuscript Author Manuscript Author Manuscript

Passive RFID applications using the RSSI ranging have mainly two different approaches, received signal strength (RSS) mapping and propagation modeling. In the RSS mapping method, reference tags are deployed in the area of interest. As the locations of the reference tags are known, k-Nearest Neighbors (kNN) algorithm is used to find the most close location for activity and motion recognition. Because reference tags can be placed mostly on the floor or walls this method only works for objects in the same plane as in reference tags and requires to collect manually the information of a number of reference tags. The other method is propagation modeling. This method is based on a propagation function of RSS versus distance. The distance between the reader antenna and the tag is determined by comparing RSS with the power function of distance. However a study [19] of wave propagation and backscatter communication link showed that a simple statistical channel model in general does not hold for indoor propagation due to multipath fading. They measured backscatter signal of RFID tags using a network analyzer in an office environment. We present the process of the raw signals to produce one statistical model.

In hospital settings for context-aware systems, some of studies used passive RFID tags to detect the presence of medical staff and objects [2], phase of surgical operation [15], nursing activity [16], and clinical intervention [14] but they detect only the presence of tags in their applications without detecting the movement of objects. When it comes to distinguishing if objects are used or not, there is no way to detect it. There are some studies on detecting the movement of RFID tagged objects. A study [5] uses sliding windows and sample mean comparison with tag's read rates instead of RSSI. With experimental scenarios they shows, an accuracy of 94% for stationary objects without human presence and moving around the area of interest but the algorithm works poorly for moving objects showing 40–65% accuracy. Another study [8] uses a sliding window, a basic HMM and data interpolation and achieves an accuracy of 80% with people moving around the area of interest.

To increase the accuracy for crowded surroundings, we propose a novel method of constructing Markov model classifier with continuous observations (RSSI) that can be trained for surroundings. Instead of using sliding window, we develop motion-transition finder for exact detection time and frame based data segmentation to provide un-correlated observations to the HMM classifier. To statically deal with continuous observations and reduce the variances of noisy RSSI, we investigate distributions, read rates, query missing rates of RSSI and then develop RSSI preprocessor. Our approach achieves an accuracy of 89.5% with four people moving from actual medical activities. Novel designs of HMM classifier and RSSI preprocessor maximizes the system accuracy in dynamic settings with human moving and improves by about 10.8% in crowded settings compared to a naive HMM.

3. Building the motion detection system

Our motion detection system is based on an HMM classifier that makes the classification of the tagged object states as "moving" or "stationary" with RSSI from a tag. Our method for motion detection relies on detecting the change of RSSI due to object relocation. To use the RSSI data for accurate detection of tagged-object movement, we first investigate the effects of multiple-tags interrogation and query-missing rate with respect to RSSI read rates and

Author Manuscript Author Manuscript Author Manuscript Author Manuscript

distributions of measured RSSI data for statistical processing. We then construct Markov models with continuous observations including RSSI preprocessor, frame-based RSSI data segmentation and motion-transition finder.

3.1. Effects of varying tag-set size on RSSI read rates

We studied the effects of different tag-set sizes on read rates and query-missing rates (Eq. 1) because we are tracking multiple objects in the area of interest simultaneously. We used an Alien Technology reader that provides RSSI in a 16-bit resolution, covering a maximum read range of 11 m. Based on observations of our target domain (trauma resuscitation), we found that up to ten tagged objects can be used simultaneously in the work area (patient bed). Many more tagged objects may be present in the room, but are normally kept outside of the work area to avoid clutter. Therefore, relatively a small number of objects are within the coverage of antennas focused on the work area. EPC Class-1 Generation-2 standard [17] supports a multi-access method for multiple-tags interrogation using a variation of slotted Aloha protocol [18]. The read rate is the number of tag interrogations per second. Queries might be missed because of collisions when multiple tags respond simultaneously and errors in wireless backscatter communication.

$$\text{Query}-\text{missing rate} = \frac{\text{The number of missing responds from the tag}}{\text{The number of Query trials by the reader}} \quad (1)$$

We dispersed a set of tags randomly in the area of interest (around 2 m from the reader antenna), aligned tag antennas parallel to the reader antenna to maximize the read rate, and left the tags stationary. The reader was commanded 1000 times to interrogate all tags within the range. As the tag-set size increased, the total number of reads per second initially increased, but then decreased around the tag-set size of 30, while the read rate per single tag monotonously decreased (Fig. 1). We observed a decrease from 30.8 interrogations per second with a single tag to 14.2 per second with 10 tags. Query-missing rates for tagset sizes up to 10 tags appeared not to depend on the tag-set size and remained below 3% (see Fig. 1, units on the right side of the chart). Reading rates for larger tag-set sizes, with 50, 100 or more tags, are very low, but as noted earlier, such large tag-sets usually do not appear within the work area. This results show that how many RSSI data can be obtained with varying tag-set size in a fixed time period.

3.2. RSSI preprocessor

Because RSSI is an observation of our classifier system, a statistical model of RSSI is required to attain emission probabilities of a number of the different observations. Another required property of RSSI preprocessor is to reduce the distribution of noisy RSSI to provide more accurate information on RSSI to the classifier. We first investigated the distributions and variances of measured RSSI data and then designed RSSI preprocessor. RSSI is a power-strength measurement of the received radio signal from a tag at the receiver device. Indoor radio propagation does not fit one statistical model and RF signal distributions at different locations are essentially unpredictable [19]. RSSI also relies on the weak backscattered signal power that is easily affected by the thermal noise at the receiver side

Author Manuscript Author Manuscript Author Manuscript Author Manuscript

and interfered by surroundings such as furniture and human. As a result, the distribution of practically measured RSSI values has a considerably large variance [7,20], which results in inherently low accuracies for RSSI-based classifications [21,22]. Fig. 2 shows distributions of RSSI values at different locations in the area of interest. Those distributions are widely different and relatively large. With Gaussian distribution approximation, the standard deviations varied between 9.6% and 21.0% of the mean, and the average of their standard deviations was 15.8% of the mean.

In practice, two sets of RSSI data taken at two adjacent locations largely overlap because of noisy RSSI characteristics. When mapping RSSI values with respect to tag's location, such overlap results in detection errors and inability to distinguish the differences in RSSI. Fig. 3(a) shows two measured RSSI data distributions, each averaged over 18 locations. The first distribution is from 18 locations (some of which shown in Fig. 2), and the second distribution is from adjacent 18 locations that are each 5 cm apart from the original 18 locations. The overlapped area is 38%, which will be the error rate of distinguishing RSSI values from two location.

To minimize variances of measured RSSI distributions and to obtain a unique distribution, we applied the Central Limit Theorem (CLT) as a RSSI preprocessor. The CLT allows obtaining accurate approximations to the Gaussian distribution associated with sums of random variables [23]. As the sample size N increases (typically $N \geq 30$), the distribution of the sample averages, $\bar{x}$, converges to the normal distribution with $\mu_{\bar{x}} = \mu_x$, $\sigma_{\bar{x}}^2 = \frac{1}{N}\sigma_x^2$ [24]:

where $x_1, \ldots, x_N$ are random variable samples with mean μ_x and variance σ_x^2. Another property of the sample average $\bar{x}$ is to reduce the variance by a factor of N. With increasing sample size N the RSSI variance decreases at a rate of $1/N$ [23]. However the sample size N needs to be balanced because short RSSI transitions from fast movements might be averaged out. We found that the minimum required distance for detecting object's motion is 5 cm by observing trauma resuscitations which is our application domain. With setting a condition that the overlap of processed RSSI distributions at two 5-cm-apart locations is close to zero (< 1%) we determined that the minimum sample size N equals 110 by calculating the overlap with processed RSSI. Fig. 3(b) shows that the overlapped processed RSSI values are 0.88% with the sample size 110. The smallest read rate for the tag-set size up to 10 is 14 reads/s (Fig. 1), so approximately 8 s are needed to read at least 110 samples. Therefore, we used an 8-s window for RSSI preprocessor. In the cases of fewer than 10 tags in the range there should be > 110 samples in an 8-s window and this will results in smaller overlap areas than that from 110 samples. Fig. 4 shows the processed RSSI distributions with the sample size of 110. Unlike the measured RSSI distributions (Fig. 2), the processed RSSI distributions at all locations make very close approximations to the Gaussian distribution, because of the CLT. The standard deviations of the estimated RSSI data are between 0.8% and 5.8% of the mean, an average of 2.3%. The estimator reduces the standard deviation of measured RSSI to 14.6%.

Author Manuscript Author Manuscript Author Manuscript Author Manuscript

$$\bar{x} = \frac{1}{N}\sum_{i=1}^{N} x_i \quad (2)$$

The variance of processed RSSI is reduced to 14.6% of the variance of measured RSSI and the distribution of processed RSSI is Gaussian. We used processed RSSI for our detection system as an input.

3.3. Detection system and motion-transition finder

We used non-overlapping segments ("frames") (Fig. 5) of processed RSSI as the observations to an HMM classifier, which makes decisions at each frame-time instant. Then, motion-transition finder searches within the selected frame for the exact time of transition from stationary to moving state. In contrast to frame-based segmentation, a sliding-window method (Fig. 6) can makes decisions at each sample time instant. It, however, shares most of the data within the adjacent windows and produces highly correlated information, making it hard to distinguish the differences between two consecutive windows. We classify frame-based segments as stationary/moving and use motion-transition finder to detect the exact time of the movement.

After an HMM classifier marks each frame with either "moving" or "stationary" state, motion-transition finder searches for the exact start and end time of state transition. Fig. 7 shows a set of frames used by motion-transition finder, with "stationary" frames at the start and end of the set, and one or more "moving" frames are in between. We use three line segments for curve fitting, because in stationary states the processed RSSI can be fitted with a horizontal line, and we observed that state transitions occur linearly between the steady states (see examples later in Figs. 11 – 13). The first segment is a horizontal line corresponding to the mean value of the first stationary frame. The end line segment is also a horizontal line at the mean value of the end stationary frame. The middle segment is a line connecting the horizontal lines representing the moving states. From potentially many middle segments, we choose the line that fits the best the processed RSSI data. The endpoints of this middle segment indicate the exact start and end times (in seconds) of the state transition (i.e., the beginning and the end of object movement).

We set the frame size to 2 s, and this size allows detecting any duration of RSSI change that remains in the output of the RSSI preprocessor. If the frame size were too large, the short durations of RSSI changes would be averaged out. Conversely, if the frame size were too small, the detection system would become subject to noise and interference. We observed object motion in trauma resuscitations and found that the shortest duration of object relocation is 2 s.

3.4. HMM classifier

3.4.1. Naive hidden Markov model (NHMM)—We first designed a NHMM (Fig. 8(a)) that makes decisions whether the tagged object is moving or stationary and then introduced Augmented hidden Markov model (AHMM) and Simplified AHMM (SAHMM). Given NHMM, the Viterbi Algorithm [25] is used to find the most likely state sequence

Author Manuscript Author Manuscript Author Manuscript Author Manuscript

through the trellis (Fig. 8(b)) by maximizing the probability of the most probable state sequence (Eqs. 3–5).

$$v_\theta(1) = P(o_t|\theta) \cdot \pi_\theta(Initialization) \quad (3)$$

$$v_\theta(t) = v_\theta(t-1) \cdot P(o_t|\theta) \cdot a_{i,\theta} \quad (4)$$

$$q(t) = \arg\max_\theta v_\theta(t) \quad (5)$$

where $1 \le t \le T$, o_t = observation, θ, i = {stationary state, moving state}, π_θ = initial probabilities of θ, $a_{i,\theta}$ = probabilities of transitioning from i to θ, and the most likely state sequence = $q(t)$.

All the parameters of NHMM are defined and explained as follows.

1) Observations.: Our system is based on RSSI which can vary with diversity of transmitted power, reader antenna gain and tag antenna gain associated with device hardware. Those devices' diversity causes extra amplitude values in RSSI measurement. By differentiating RSSI values on a frame basis, we eliminate the common extra amplitude of each frame RSSI introduced by the diversity. For instance, the difference of sample means of RSSI values from a stationary tag tends to be zero regardless of extra RSSI values from the device diversity. Thus, we define NHMM observations to be the difference between the mean RSSI values of the current frame and the predecessor frame:

$$o_t = m_t - m_{t-1},\ t \ge 2 \quad (6)$$

where t is the frame based time and m_t is the mean of processed RSSI values in frame t.

2) The emission probabilities in the states.: Because processed RSSI is a Gaussian random variable, any liner transformation of processed RSSI produces another Gaussian random variable. Therefore m_t is Gaussian $(\mu_{m_t}, \sigma_{m_t})$, m_{t-1} is Gaussian $(\mu_{m_{t-1}}, \sigma_{m_{t-1}})$, and o_t is Gaussian$(\mu_{o_t} = \mu_{m_t} - \mu_{m_{t-1}}, \sigma_{o_t} = \sigma_{m_t} + \sigma_{m_{t-1}})$.

Using the Gaussian distribution of the observations the emission probabilities of observations in the stationary state and moving state are defined:

Author Manuscript Author Manuscript Author Manuscript Author Manuscript

An emission probability of observation o_t in the stationary state denoted by $I(o_t|\theta_{stationary})$ follows Gaussian($\mu_{o_t} = 0, \sigma_{o_t} = \sigma_{m_t} + \sigma_{m_{t-1}}$). In the stationary state, μ_{O_t} is zero because $\mu_{m_t} = \mu_{m_{t-1}}$.

An emission probability of observation o_t in the moving state denoted by $I(o_t|\theta_{moving})$ follows Gaussian ($\mu_{o_t} = \mu_{m_t} - \mu_{m_{t-1}}, \sigma_{o_t} = \sigma_{m_t} + \sigma_{m_{t-1}}$).

The mean and standard deviation in each state are decided and optimized with training data sets.

3) Optimality criterion.: The target to detect is whether an object moving. False positive error generates false information on the motion of moving while false negative error results in losing the motion information. Both types of errors should be minimized. In our context, sizes of the positive (moving) and negative (stationary) classes are different. The number of the stationary states overruns the number of the moving states since objects are more likely in stationary. We use Matthew's Correlation Coefficient (MCC) as a optimality criterion for our HMM classifier because it works with skewed class imbalance and takes into account both false positive and false negative errors [26].

4) Initial and transition probability distributions.: By supervised training, initial and transition probabilities are learned from respective frequencies of state transitions from training data sets.

3.4.2. Augmented hidden Markov model (AHMM)—With the fact that reducing the variance of a RSSI distribution contributes to lowering the overlapping area of distributions of different RSSI sets which results in errors (Fig. 3), we design AHMM (Fig. 9) to reduce the variance of the observation (Eq. 6) in the stationary states. In a period of frames in which the stationary state keeps continuing, each mean of the frame data converges the mean of the period data and m_{t-1} can be replaced with $\hat{m}_{t-1}$. The observation of continuing stationary states is:

$$o_t = m_t - \hat{m}_{t-1} \quad (7)$$

$$\hat{m}_{t-1} = \frac{1}{k}\sum_{i=0}^{k-1} m_{(t-1)-i} \quad (8)$$

where k is the number of continuing stationary states.

By processing multiple stationary frames, the variance of averaged $\hat{m}_{t-1}$ is reduced, so the observation variance in continuing stationary states, $\sigma^2_{o_t}\left(= \sigma^2_{m_t} + \sigma^2_{\hat{m}_{t-1}}\right)$ becomes smaller

Author Manuscript Author Manuscript Author Manuscript Author Manuscript

than the observation distribution in Eq. 6. By the CLT, upon further increasing k, $\sigma^2_{\hat{m}_{t-1}}$ converges zero, so the observation distribution in continuing stationary states can be reduced to ${\sigma_{m_t}}^2$. Fig. 10 shows an experimental result. The stationary state continues, on average, variances of $\hat{m}_{t-1}$ are reducing 2 quickly below $0.15 \times {\sigma_{m_{t-1}}}^2$ at 8th continuing stationary state. The used RSSI values are taken ten thousand times from a stationary tag at the nine locations (Fig. 2).

Fig. 9 shows the states of AHMM to reduce the observation variance in the stationary states. In each stationary state, $\hat{m}_{t-1}$ is updated using Eq. 8 and results in reduced variances of the observation.

3.4.3. Simplified AHMM (SAHMM)—The critical impediment in realization of AHMM (Fig. 9) is to train a number of states since supervised training is used in our context. To yield stable parameters of all the fine stationary states, the training requires much more training data and ground truths involving a great amount of fine handwork. Thus, we simplify a number of the stationary states of AHMM to a single stationary state for feasible training while keep the property of reducing the observation distribution. Thus SAHMM has one stationary state and one moving state as in NHMM but uses the same observations of AHMM.

1) Observations.: We use the observations to AHMM defined in Eqs. 7 and 8 from the previous section.

As the stationary state continues, $\hat{m}_{t-1}$ can be determined with m_{t-1} and $\hat{m}_{t-2}$ that is from the previous stationary state, without using all the history of m:

$$\hat{m}_{t-1} = \left(\hat{m}_{t-2} \times (k-1) + m_{n-1}\right)/k \quad (9)$$

where k is the number of continuing stationary states (Fig. 9).

Thus the observation to SHMM can be realized in a functional form with m_t, m_{t-1} and $\hat{m}_{t-2}$ without using additional memories and further history of data.

2) Emission probabilities of the states.: Emission probabilities $I(O|\theta_{moving})$ and $I(O|\theta_{stationary})$ remain unchanged as in AHMM, while with training data sets, the variance of the emission probabilities is trained.

3) Initial and transition probability distributions.: By supervised training, those distributions also remain unchanged as in NHMM.

3.4.4. Overall detection system for crowded indoors scenarios—In this section, we show how each component of the detection system works with three experimental scenarios (Figs. 11 – 13). Those scenarios consist of the cases of four people moving

Author Manuscript Author Manuscript Author Manuscript Author Manuscript

around, one person moving and monotonous increment of RSSI with respect to human interference and detectable RSSI changes. Our area of interest is the patient bed in a trauma resuscitation room, surrounded by a medical team treating the patient (Fig. 14). In the scenario of four people moving around the bed, much bigger ripples in stationary-state RSSI values were observed compared to the scenario with one person moving (Fig. 12). NHMM and SAHMM were trained using a set of RSSI values from the first scenario (Fig. 11), and applied to all three scenarios. Because of the training set with heavy ripples, both SAHMM and NHMM might miss small changes in RSSI value (Fig. 13). Due to the reducing-variance characteristics of SAHMM, it detects all the movements in Fig. 11 except for the smallest movements (Fig. 13). NHMM, however, misses most of the smallest changes (Fig. 13).

4. Evaluation

4.1. System hardware

We installed and used commercial off-the-shelf (COTS) equipment from Alien Technology [27] and Confidex which includes two of RFID reader ALR-9900, two circularly polarized wide angle antenna ALR-8696-C and two types of passive UHF tags (ALN-9740 and Confidex Steelwave Micro II [28]). Fig. 14 shows the layout of the trauma bay with two RFID reader antennas and a patient bed. The two reader antennas point to the center of the bed from different viewing angles, which is close to perpendicular in three-dimensional space. These two antennas allow to integrate tags at all directions and also use a better RSSI set between two antennas for the case that medical staffs might obscure one of the antennas' line-of-sight RFID signals resulting in degrading signal strength and a insufficient data set in number. The RFID readers and a desktop computer are connected to a router for TCP/IP communication. The reader has a local clock and offers a timestamp with a millisecond resolution for each RSSI read. The timestamp is used for the fixed frame in time. Two different types of passive UHF tag are used for different materials of medical objects. One type is ALN-9740 for non-metallic objects, its dimensions are 98.2×12.3×0.08 mm and the read range is up to 11 m. The other type is Confidex Steelwave Micro II for metallic objects such as laryngoscope and its dimensions and read range are 38×13×4.5 mm and up to 5 m on metal. The communication protocol used between the readers and the passive tags is the EPC ClASS-1 Generation-2 standard [17].

4.2. Passive medical objects tagged

Nine passive medical objects are selected and tagged, mostly used on and near to the patient bed in resuscitations such as bag valve mask (BVM), collar, laryngoscope, ETtube (ETT), Stethoscope, Fluid bag, IV start kit, IV tubing, and thermometer (Fig. 15).

4.3. Data collection and ground truth data

With the deployment of the RFID system, RFID data and surveil-lance video are recorded during 28 simulated resuscitations, each about 20 min long. The recorded surveillance videos are used to make ground truth data. There are four resuscitation scenarios and each one was preformed seven times by different trauma teams. The average number of medical staffs moving around the area of interest is four in the resuscitations. The scenarios include High-speed motor vehicle collision, pedestrian struck at approx 20 mph, restrained

Author Manuscript Author Manuscript Author Manuscript Author Manuscript

passenger in head-on collision and pedestrian struck in a parking lot, involving the nine passive medical objects for treatments such as endotracheal intubation, administration of fluids and mediations, temperature control and ET-tube insertion.

4.4. Experimental results

From the 28 resuscitations, 20 resuscitations, each five resuscitations from four different scenarios, are taken at random and used for training NHMM and SAHMM and 8 resuscitations are used for evaluations. The results are shown in Fig. 16. Each of tagged objects has distinctive usage and moving characteristic so detection accuracies are slightly different. RSSI data are extracted according to tag's ID and the antenna and feed to the detection system with distinct parameters. Data from different antennas might produce contrastive detections. Then the detection with a higher data rate is taken because better signal reception results in higher data rates.

SAHMM shows 10.8% improvement in accuracy on average compared to NHMM. The object movement is identified with 89.5% accuracy on average by SAHMM. The stethoscope shows the lowest accuracy of 72.4% from the fact that most radio signals from the tag are absorbed by human body resulting in low data rates. In general, medical staffs carry stethoscopes on the chest or around the neck when not in-use so human body can absorbs both signals from a reader antenna and backscattered signals from a tag attached on the stethoscope. This absorbing effect results in missing RSSI reads and a low accuracy.

5. Conclusion

In this paper, we present a detection system for providing information on moving and stationary motion of passive medical objects being used in the area of interest using UHF RFID technology. The novel methods to achieve a high accuracy are RSSI preprocessor, SAHMM classifier, frame based segmentation and motion-transition finder. The RSSI preprocessor reduces the variance of RSSI distribution introduced by the thermal noise and makes accurate approximations to the Gaussian distribution. To detect tagged object's motion, we use RSSI change of the tag based on its relocation with frame based segmentation of RSSI data. The motion-transition finder determines the exact movement time within a frame based period. SAHMM is trained for crowded settings with human moving and the movement and in-use frequency of each tagged object to maximize its detection accuracy tackling environmental interference. Proposed SAHMM increases the detection accuracy by 10.8% compared to NHMM. Our system is evaluated with RSSI data recorded in an actual trauma bay in simulated resuscitations performed by trauma teams and shows 89.5% accuracy with human moving around the area of interest. From this result we expect that passive UHF RFID technology can be a method of providing information on both the movement and identification of passive medical objects for context-aware systems.

References

[1]. Turaga P, Chellappa R, Subrahmanian V, Udrea O, Machine recognition of human activities: a survey, IEEE Trans. Circuits Syst. Video Technol 18 (11) (2008) 1473–1488.

[2]. Agarwal S, Joshi A, Finin T, Yesha Y, Ganous T, A pervasive computing system for the operating room of the future, Mobile Net. Appl 12 (2–3) (2007) 215–228.

Author Manuscript Author Manuscript Author Manuscript Author Manuscript

[3]. Parlak S, Ayyer S, Liu YY, Marsic I, Design and evaluation of RFID deployments in a trauma resuscitation bay, IEEE J. Biomed. and Health Inform 18 (3) (2014) 1091–1097. [PubMed: 24108484]

[4]. Parlak S, Sarcevic A, Marsic I, Burd RS, Introducing RFID technology in dynamic and time-critical settings: requirements and challenges, J. Biomed. Inform 45 (5) (2012) 958–974. [PubMed: 22531830]

[5]. Jiang B, Fishkin KP, Roy S, Philipose M, Unobtrusive long-range detection of passive RFID tag motion, IEEE Trans. Instrum. Meas 55 (1) (2006) 187–196.

[6]. Banerjee SR, Jesme R, Sainati RA, Performance analysis of short range UHF propagation as applicable to passive RFID, Proc. IEEE RFID Conf (2007) 30–36.

[7]. Brchan JL, Zhao L, Wu J, Williams RE, Pérez LC, A real-time RFID localization experiment using propagation models, 2012 IEEE International Conference on, 2012.

[8]. Parlak S, Marsic I, Detecting object motion using passive RFID: a trauma resuscitation case study, IEEE Trans. Instrum. Meas 62 (9) (2013) 2430–2437.

[9]. Yang L, Chen Y, Li XY, Xiao C, Li M, Liu Y, Tagoram: real-time tracking of mobile RFID tags to high precision using COTS devices, Proc. 20th Annual ACM Int'l Conf. Mobile Computing and Networking, 2014, pp. 237–248.

[10]. Zhang P, Gummeson J, Ganesan D, Blink: A high throughput link layer for backscatter communication, Proc. 10th ACM Int'l Conf. Mobile Sys., Applic's, and Services, pp.99–112, 2012.

[11]. Poppe R, A survey on vision-based human action recognition, Image Vis. Comput 28 (6) (2010) 976–990.

[12]. Weinland D, Ronfard R, Boyer E, A survey of vision-based methods for action representation, segmentation and recognition, Comput. Vis. Image Underst 115 (2) (2011) 224–241.

[13]. Khan AM, Lee YK, Lee SY, Kim TS, A triaxial accelerometer-based physical-activity recognition via augmented-signal features and a hierarchical recognizer, IEEE Trans. Info. Tech. Biomed 14 (5) (2010) 1166–1172.

[14]. Ohashi K, Ota S, Ohno-Machado L, Tanaka H, Smart medical environment at the point of care: auto-tracking clinical interventions at the bed side using RFID technology, Comput. Biol. Med 40 (6) (2010) 545–554. [PubMed: 20471637]

[15]. Bardram JE, Doryab A, Jensen RM, Lange PM, Nielsen KL, Petersen ST, Phase recognition during surgical procedures using embedded and body-worn sensors, IEEE Int'l Conf. Pervasive Comput. Commun. (PerCom) (3 2011) 45–53.

[16]. Inomata T, Naya F, Kuwahara N, Hattori F, Kogure K, Activity recognition from interactions with objects using dynamic bayesian network, Proc. 3rd ACM Int'l Workshop Context-Awareness for Self-Managing Sys, pp.39–42, 5 2009.

[17]. GS1 Standards, http://www.gs1.org/epc-rfid.

[18]. Robert LG, Aloha packet system with and without slots and capture, ACM SIGCOMM Comput. Commun. Rev 5 (2) (1975) 28–42.

[19]. Mayer LW, Wrulich M, Caban S, Measurements and channel modeling for short range indoor UHF applications, Proc. Eur. Conf. Antennas Propag (2006) 1–5.

[20]. Tan SY, Tan HS, Improved three dimensional ray tracing technique for micro-cellular propagation models, Electronics Letters, vol.31, no.17, pp.1503–1505, 17th, 8 1995.

[21]. Joho D, Plagemann C, Burgard W, Modeling RFID signal strength and tag detection for localization and mapping, Proc. IEEE Int'l Conf. Robot. Autom. (2009) 3160–3165.

[22]. Torres-Solis J, Falk TH, Chau T, A review of indoor localization technologies: towards navigational assistance for topographical disorientation, Ambient Intell (2010) 51–84.

[23]. Yates RD, Goodman DJ, Probability and Stochastic Processes, 2nd Edition, John Wiley & Sons, Inc, 2005, pp. 257–269.

[24]. Dinov ID, Christou N, Sanchez J, Central limit theorem: New SOCR applet and demonstration activity, J. Stat. Educ 16 (2) (2008) 1–15. [PubMed: 21833159]

[25]. Forney GD, Jr., The Viterbi algorithm, Proc. IEEE 61 (3) (1973) 268–278.

Author Manuscript Author Manuscript Author Manuscript Author Manuscript

[26]. Jurman G, Riccadonna S, Furlanello C, A comparison of MCC and CEN error meaures in multi-class prediction, PLoS ONE 7 (8) (2012).

[27]. Alien Technology, http://www.alientechnology.com/.

[28]. CONFIDEX, http://www.confidex.com/.

Author Manuscript Author Manuscript Author Manuscript Author Manuscript

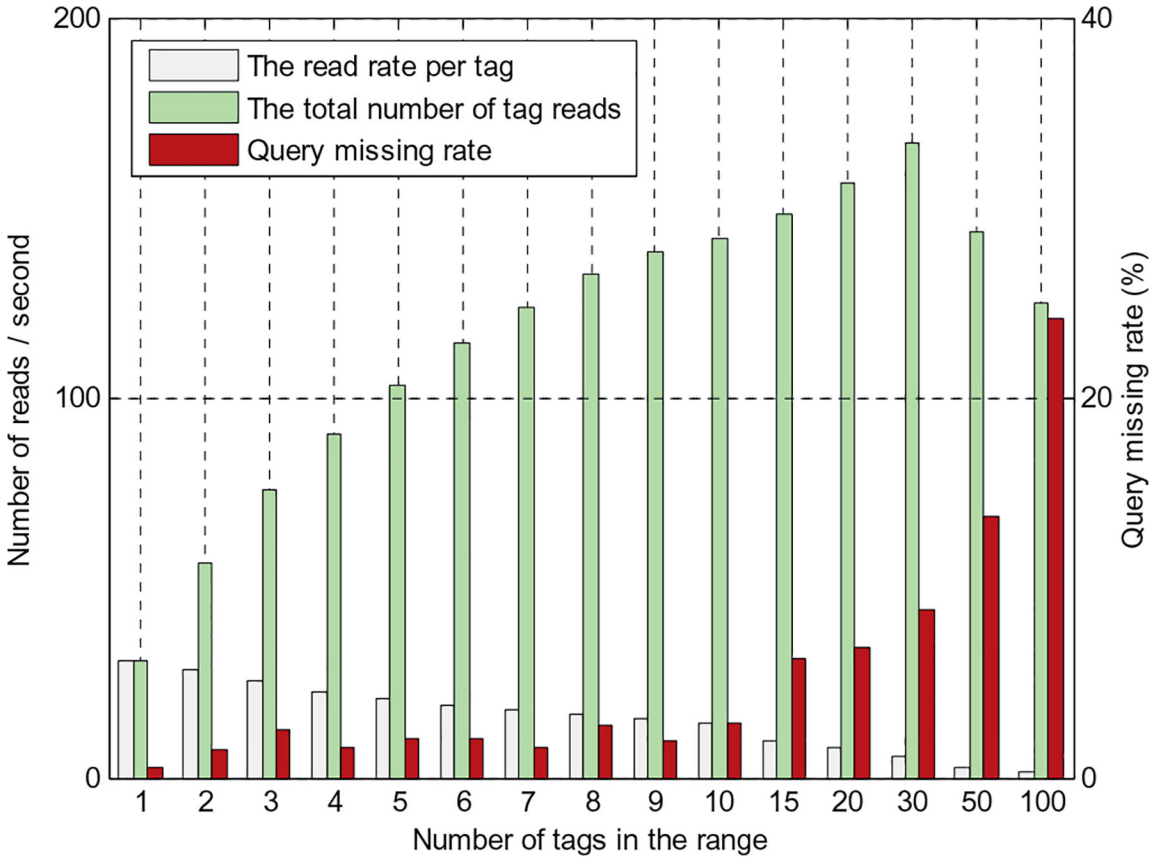

Fig. 1.

Read rates and query-missing rates according to the number of tags at around 2 m from the reader antenna. Note the read-rate units on the left side and query-missing-rate units on the right side of the chart.

Author Manuscript Author Manuscript Author Manuscript Author Manuscript

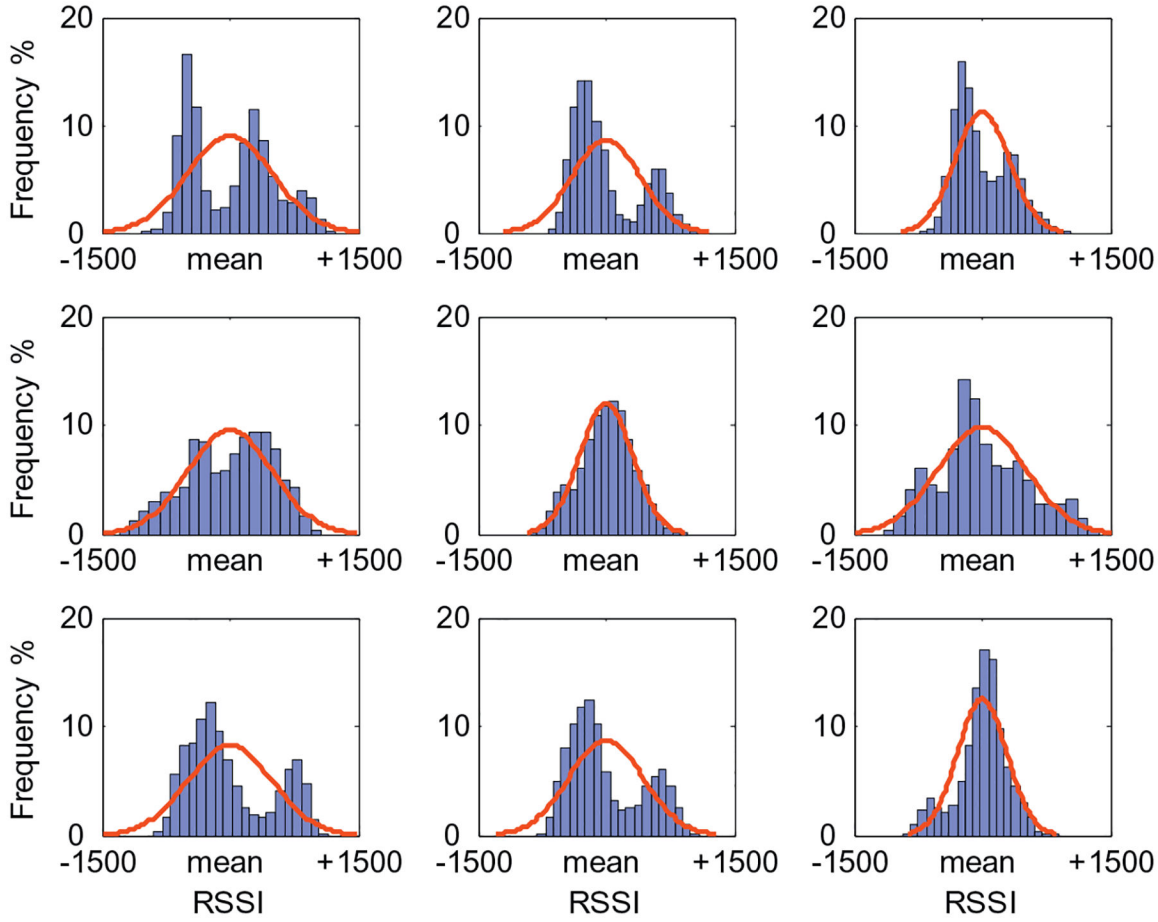

Fig. 2.

Distributions of measured RSSI at different locations in the area of interest (9 locations out of 18 are shown), where each set contains 10,000 samples. The bell curves are fitted Gaussian distributions.

Author Manuscript Author Manuscript Author Manuscript Author Manuscript

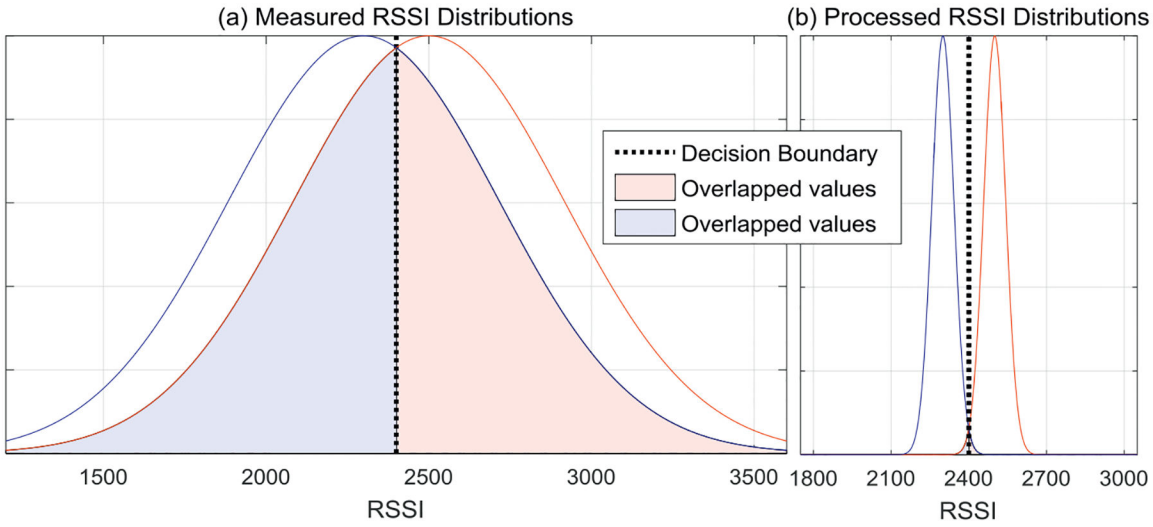

Fig. 3.

Distributions of measured RSSI and processed RSSI from 18 pairs of locations, shown as bell curves. In both charts, the left bell curve shows distribution averaged from 18 locations in Fig. 2 and the right curve shows distribution from 18 tandem locations, each 5 cm apart from the original. The decision boundary (thick dotted line) is set to be the midpoint of the means of two distributions.

(a) The measured RSSI data distributions overlap by 38%.

(b) The distributions of processed RSSI values overlap only by 0.88%.

Author Manuscript Author Manuscript Author Manuscript Author Manuscript

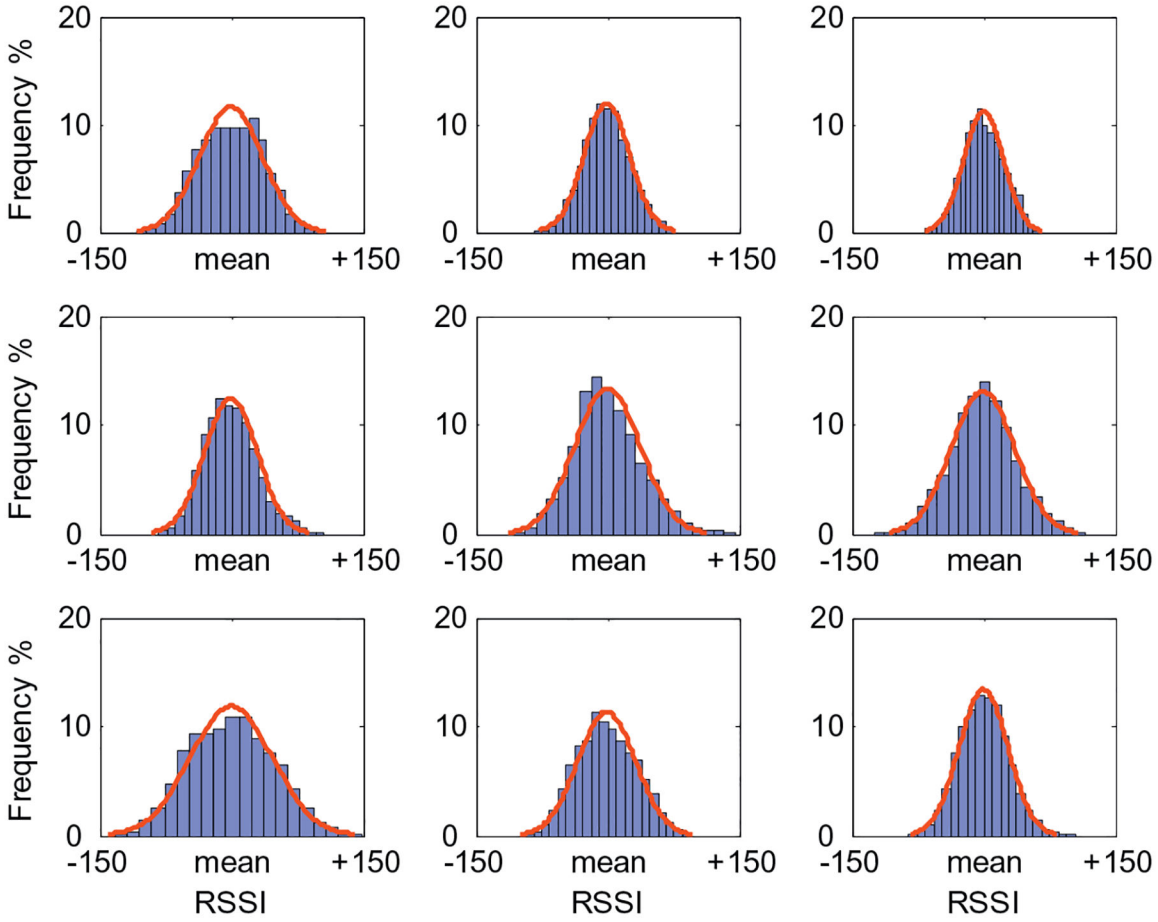

Fig. 4.

Processed RSSI distributions at the locations corresponding to those in Fig. 2 using the preprocessor with $N = 110$. The bell curves are fitted Gaussian distributions.

Author Manuscript Author Manuscript Author Manuscript Author Manuscript

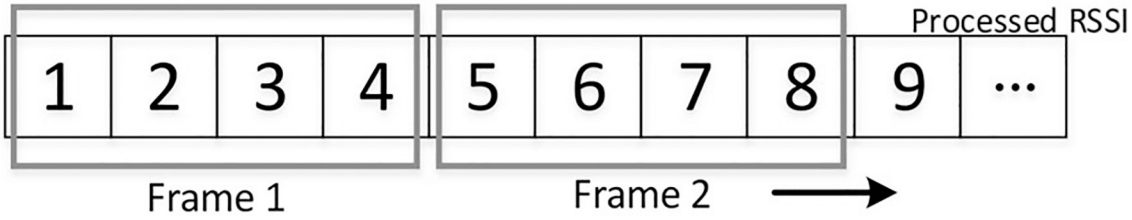

Fig. 5.
Frame based (non-overlapping) segmentation of time series data.

Author Manuscript Author Manuscript Author Manuscript Author Manuscript

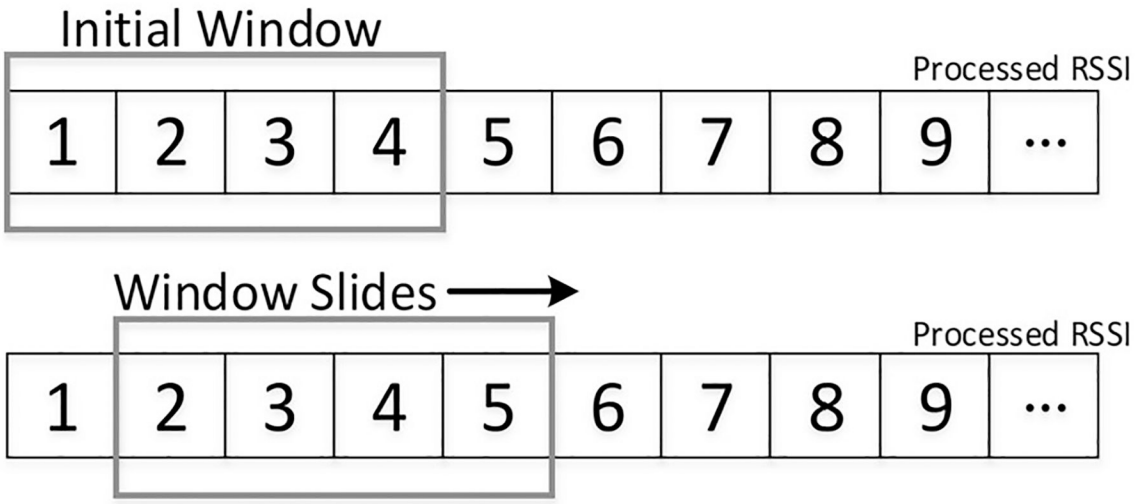

Fig. 6.
Sliding window based segmentation of time series data.

Author Manuscript Author Manuscript Author Manuscript Author Manuscript

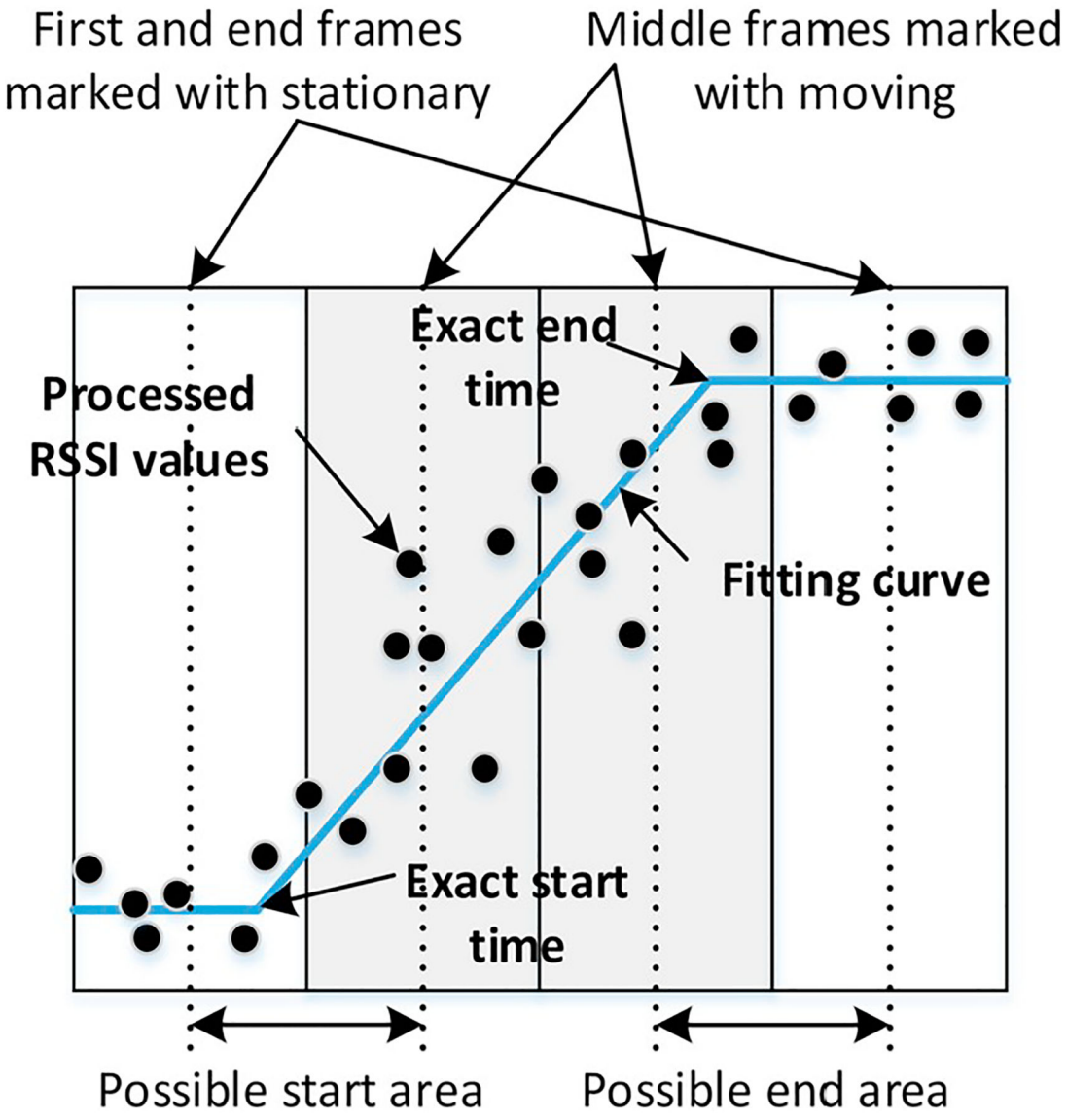

Fig. 7.
A set of frames for motion-transition finder and a fitting curve.

Author Manuscript Author Manuscript Author Manuscript Author Manuscript

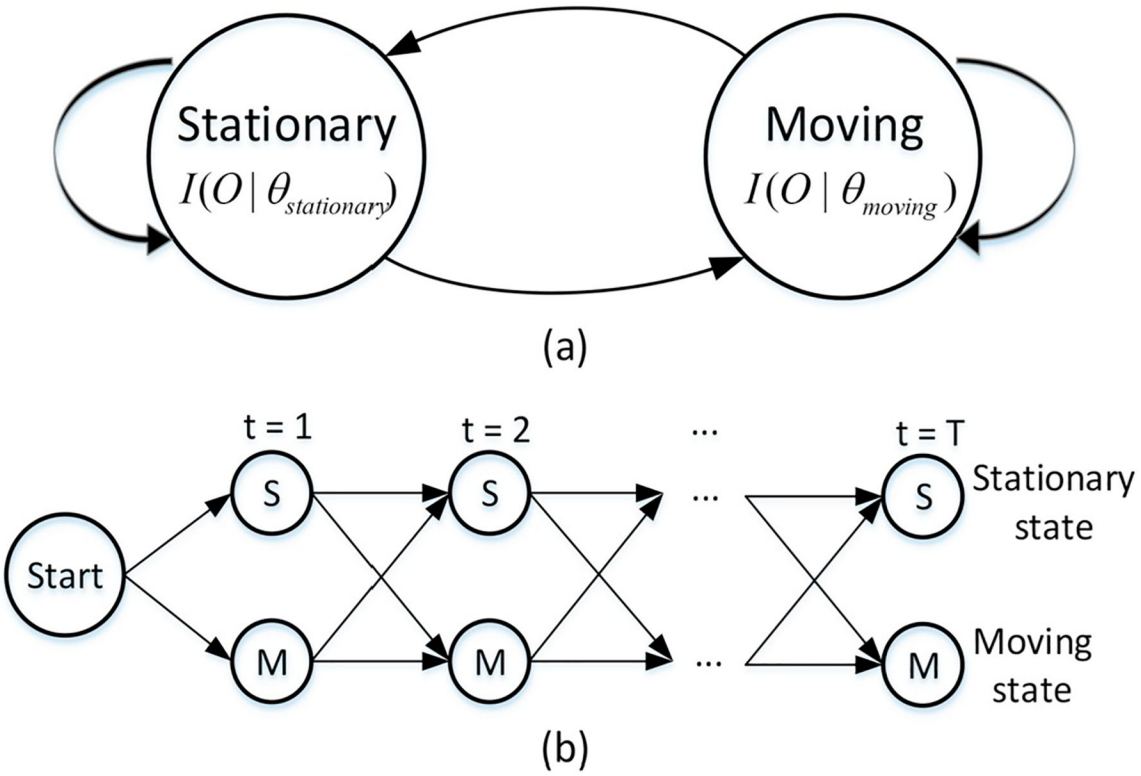

Fig. 8.

(a) State diagram of the Naive hidden Markov model; $I(x \mid \Theta)$ is the emission probability distribution where o is the observation (Eq. 6). (b) Trellis for the Viterbi Algorithm.

Author Manuscript Author Manuscript Author Manuscript Author Manuscript

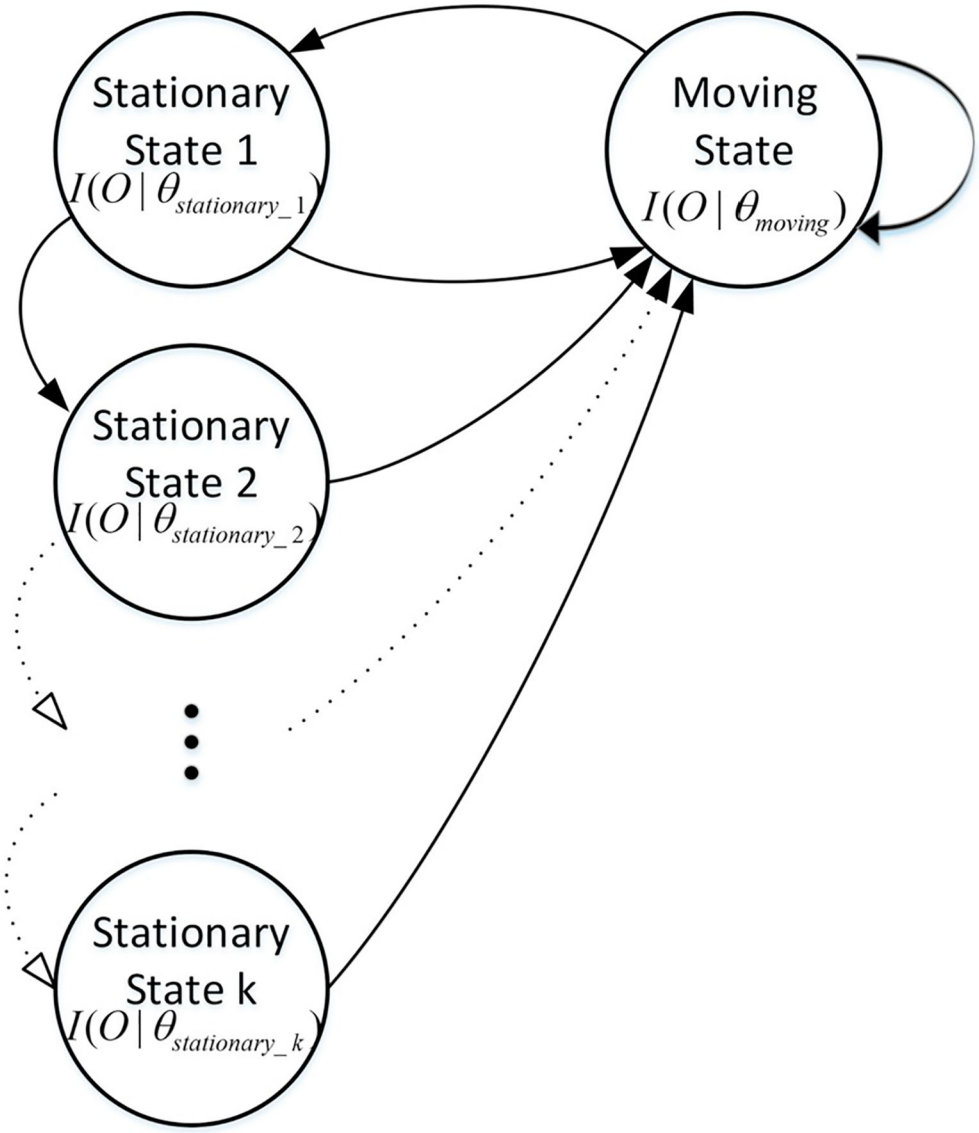

Fig. 9.
The state diagram of AHMM.

Author Manuscript Author Manuscript Author Manuscript Author Manuscript

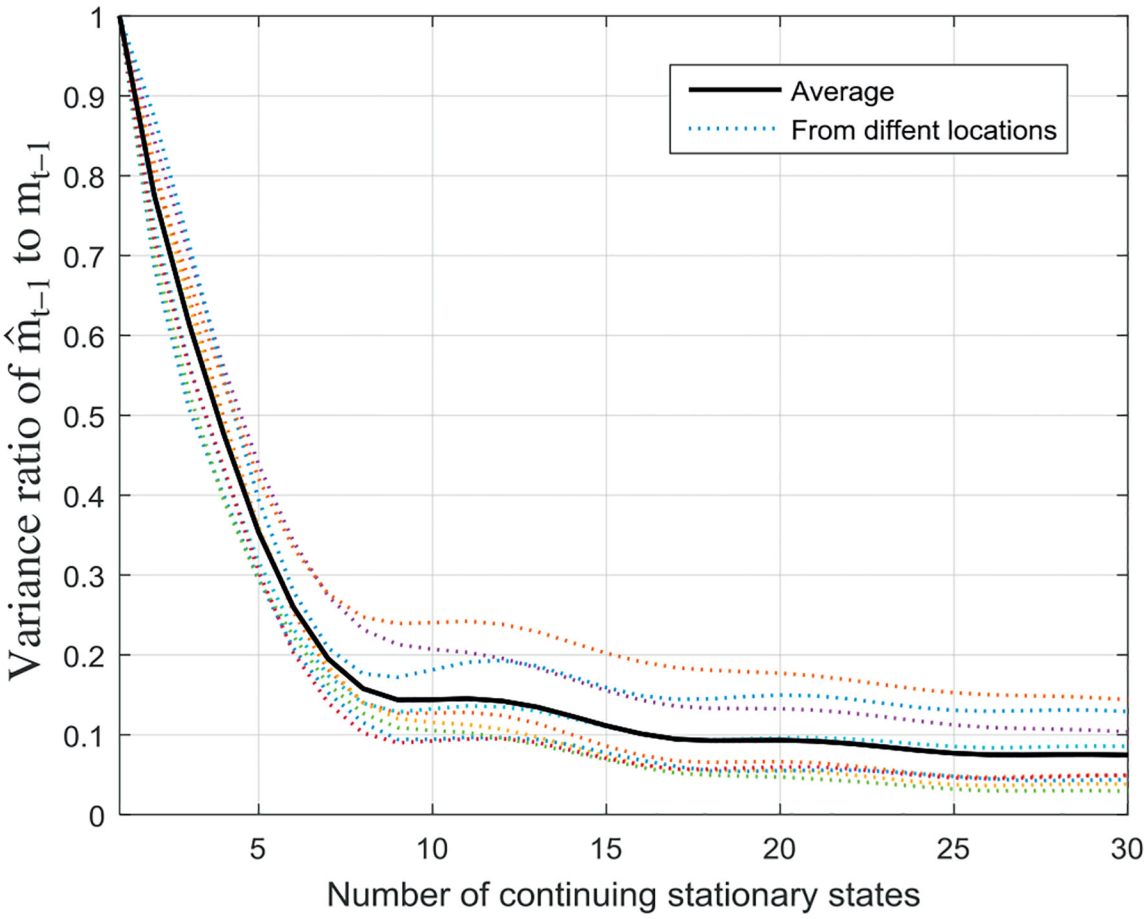

Fig. 10.

The ratio of variance of $\hat{m}_{t-1}$ to m_{t-1} as the stationary state continues. RSSI data are taken at the same nine locations as in Fig. 2.

Author Manuscript Author Manuscript Author Manuscript Author Manuscript

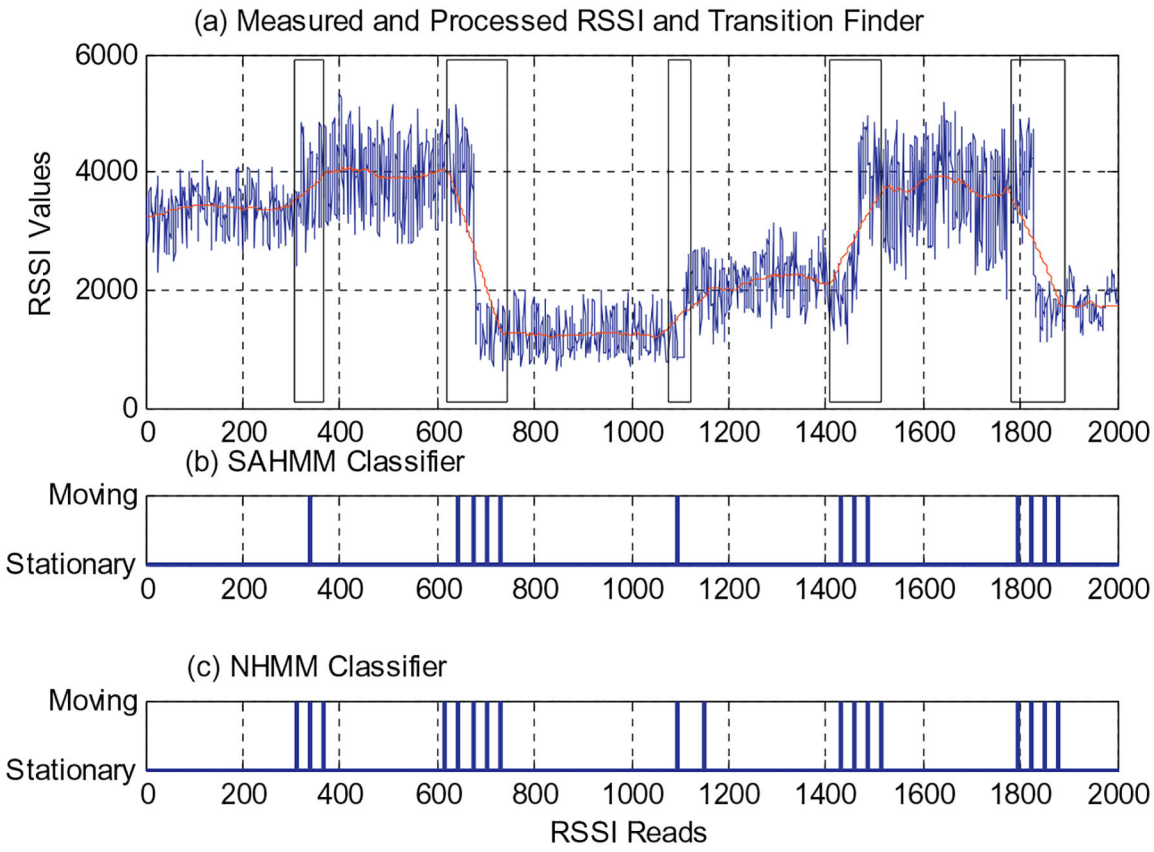

Fig. 11.

A scenario with random tag movement and four people moving randomly in the area of interest, (a) Spiky lines show measured RSSI values, the smooth line shows processed RSSI, and rectangular boxes show the exact transition times from motion-transition finder with SAHMM outputs; (b) Detection output of ASHMM; (c) Detection output of NHMM at each frame instant.

Author Manuscript Author Manuscript Author Manuscript Author Manuscript

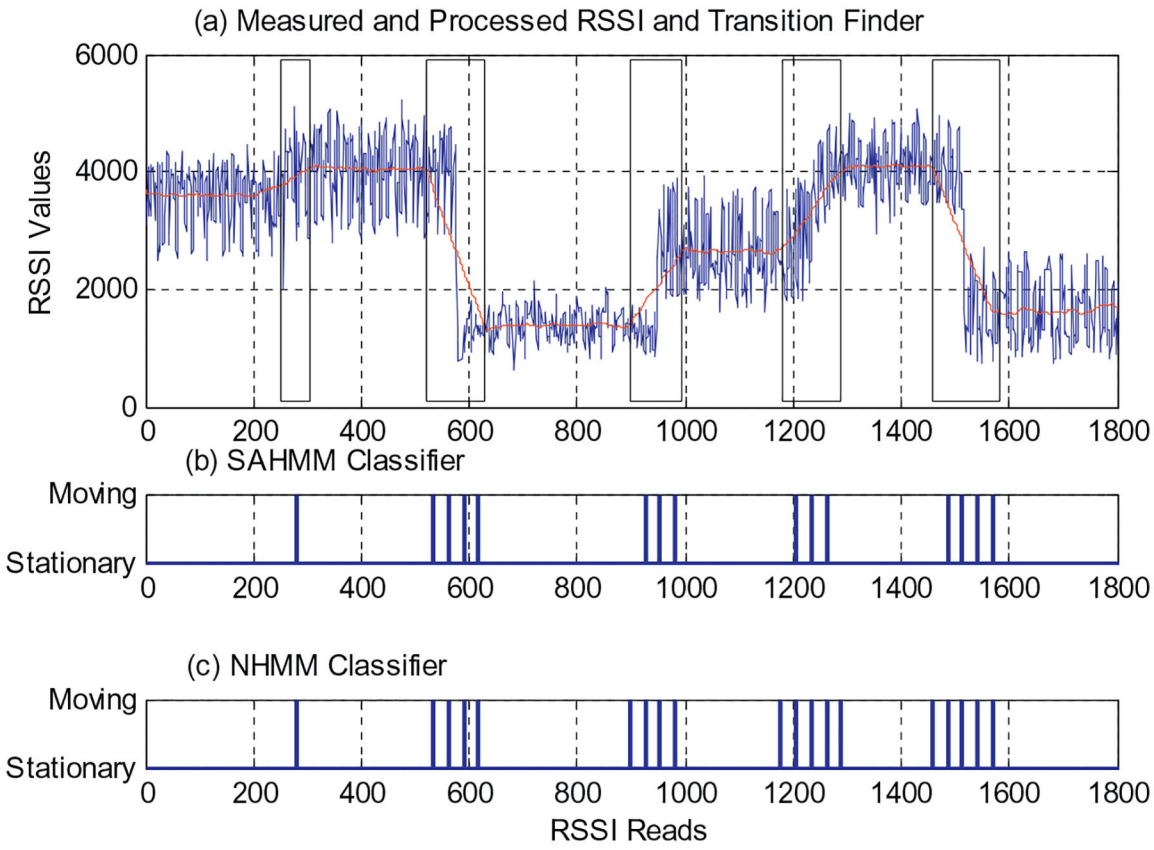

Fig. 12.

A scenario with random tag movement and one person moving in the area of interest. Charts (a) – (c) have the same meaning as in Fig. 11.

Author Manuscript Author Manuscript Author Manuscript Author Manuscript

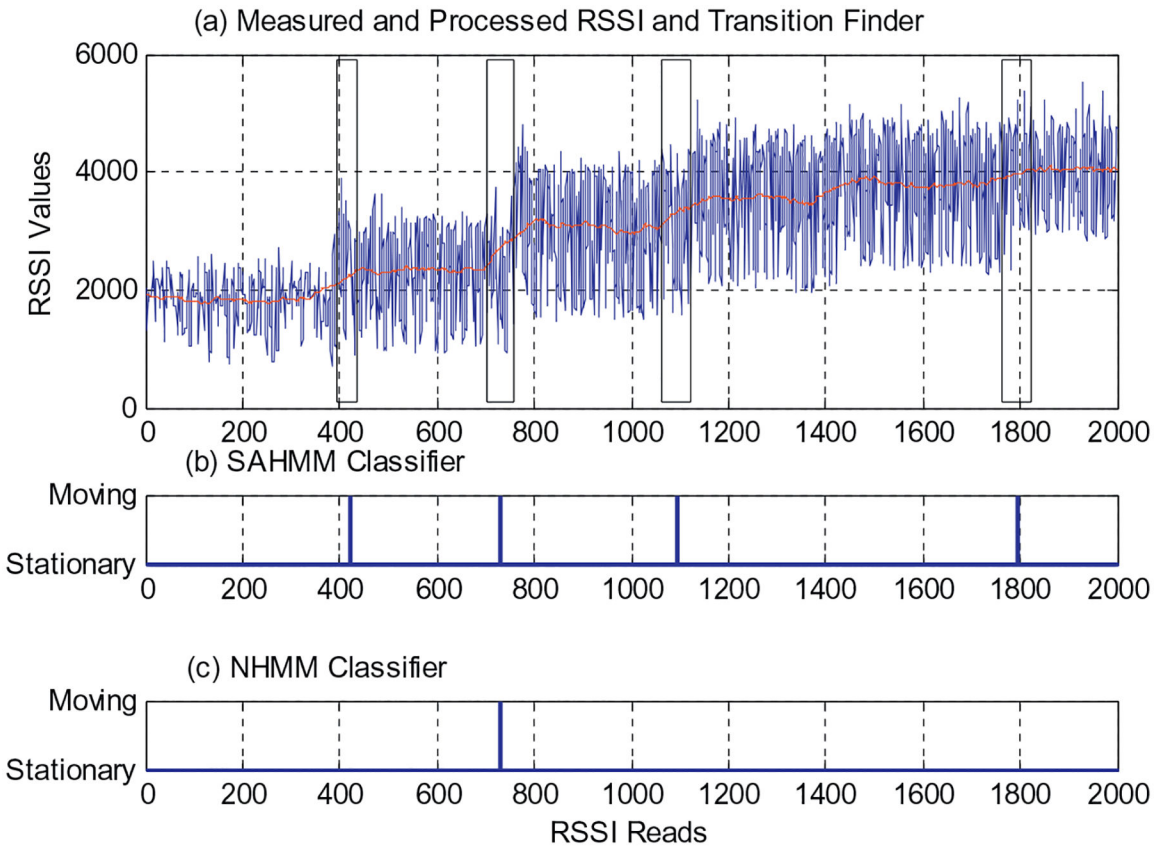

Fig. 13.

A scenario with the tag's rotating to produce small RSSI increments in monotone and one person moving in the area of interest. Charts (a) – (c) have the same meaning as in Fig. 11.

Author Manuscript Author Manuscript Author Manuscript Author Manuscript

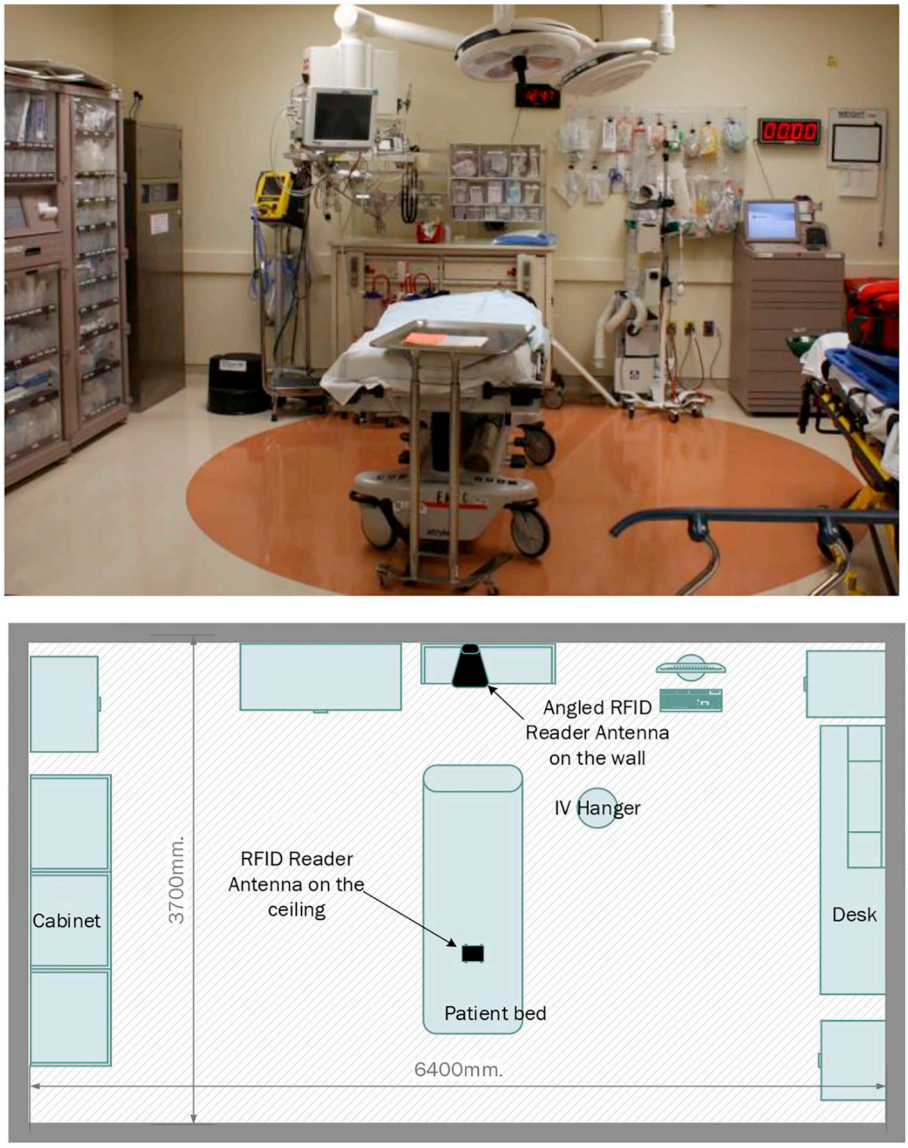

Fig. 14.
The layout and picture of the trauma bay with two RFID reader antennas and a patient bed.

Author Manuscript Author Manuscript Author Manuscript Author Manuscript

Fig. 15.
The tagged passive medical objects; from upper left, ETT, IV start kit, thermometer and stethoscope. From lower left, laryngoscope, collar, IV tubing, fluid bag and BVM.

Author Manuscript Author Manuscript Author Manuscript Author Manuscript

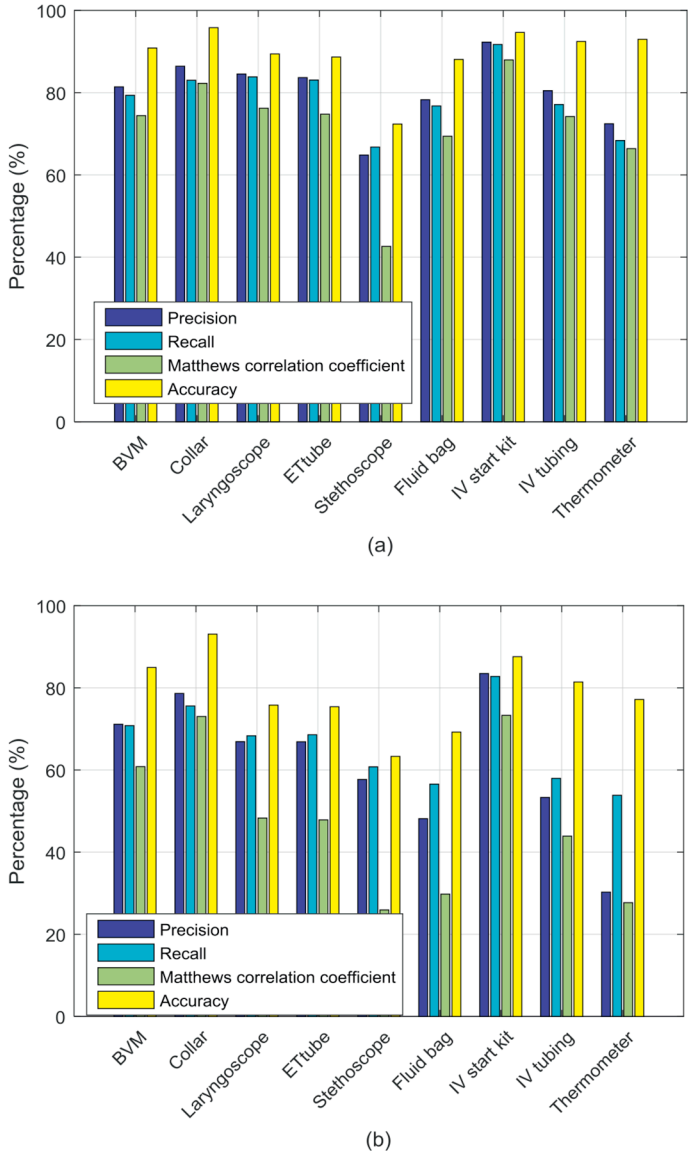

Fig. 16.

Motion detection performance of classifiers. (a) results from SAHMM. (b) results from NHMM.